Effects of two scaling exponents on biaxial deformation and mass transport of swollen elastomers

Dai Okumura [a,b*], Masahiro Mizutani [c], Hiro Tanaka [a], Makoto Uchida [d]

[a] Department of Mechanical Engineering, Osaka University,
Yamadaoka, Suita, Osaka 565-0871, Japan
[b] Department of Mechanical System Engineering, Nagoya University,
Furo-cho, Chikusa-ku, Nagoya 464-8603, Japan
[c] Department of Computational Science and Engineering, Nagoya University,
Furo-cho, Chikusa-ku, Nagoya 464-8603, Japan
[d] Department of Mechanical Engineering, Osaka City University,
Sugimoto, Sumiyoshi-ku, Osaka 558-8585, Japan
[*] Corresponding author: okumura@mech.eng.osaka-u.ac.jp

Abstract:
In this study, we investigate the effects of two scaling exponents on the biaxial deformation and mass transport of swollen elastomers. Two scaling exponents are included in an extended version of the Flory–Rehner model (Okumura et al., J. Mech. Phys. Solids, 2016); two scaling exponents are used to adjust the swelling effects on the Young's modulus and osmotic pressure of swollen elastomers, resulting in the ability to predict swelling-induced strain softening under uniaxial tensile loading. It is found that when biaxial tensile loading is given under stress control, strain softening is accelerated by increasing the biaxial stress ratio, while under strain control, the responses become more complicated, which can be interpreted by considering that Poisson's ratio at equilibrium free swelling can take negative values depending on the two scaling exponents. Further, the effect of the two scaling exponents on mass transport is discussed by analyzing the swelling kinetics of a gel layer constrained on a rigid substrate.

Keywords: Elastomers, Swelling, Constitutive modeling, Biaxial deformation, Solvent migration

1. Introduction

The Flory–Rehner (F–R) model [1] is used to describe the mechanical and swelling behavior of elastomers [2,3]. The free energy function consists of the sum of two free energies associated with polymer stretching and the mixing of polymer and solvent molecules, which are derived from the Gaussian network theory (i.e., a neo-Hookean solid model) and the Flory–Huggins solution theory, respectively. When the F–R model is assumed, the boundary value problem of swollen elastomers is equivalent to that of a hyperelastic solid [4,5], so that the F–R model is easily implemented into commercial finite element software using user-defined material subroutines. These subroutines allow researchers to perform finite element analysis of the swelling-induced surface instability of hydrogel films [6,7] and swelling-induced pattern transformation in porous gel films [4,8–11]. Further, solvent migration in the transient state can also be analyzed by introducing a diffusion model into the governing equations [12–18]. Thus, the F–R model provides a basis to interpret the mechanical behavior of swollen elastomers in both static and transient states, but it is not free from criticism.

Neo-Hookean solid models may be a poor choice to predict the stress-strain behavior of elastomers, especially at large strain and/or under biaxial deformation. When swollen elastomers are subjected to uniaxial loading, neo-Hookean solid models predict that $E = E_\mathrm{d} J^{-1/3}$ and $\sigma_\mathrm{r} = E_\mathrm{d} / 3$, where E_d and E are the Young's moduli of the dry and swollen state, respectively, J is the volume swelling ratio, and σ_r is a transformed stress referred to as the swelling reduced stress [19,20]. However, experiments show that $E = E_\mathrm{d} J^{l}$ has various values of l depending on the elastomer, and σ_r is not constant but a function of J, and, especially under tension, σ_r is also affected by stretching in the loading direction [21–23]. To overcome these problems, a neo-Hookean solid model in the F–R model can be superseded by advanced solid models, e.g., the Moony–Rivlin, Arruda–Boyce, and Ogden models [2,3,13]. Flory and Erman [24] proposed the constrained chain model, in which a neo-Hookean solid model was modified by adding terms to describe constrained chains. Drozdov and Christiansen [25,26] derived an equivalent expression of this model using stretch invariants and developed extended models by including phenomenological parameters to correctly

predict the mechanical response of hydrogels under multi-axial deformation. Generally, advanced models involve complicated strain energy functions with a substantial number of phenomenological parameters. If the parameters are fitted to a particular set of mechanical responses, there may be no guarantee that other responses can also be correctly predicted using the same parameters.

As an extended version of the scaling approach [27,28], Okumura et al. [29] extended the F–R model using two scaling exponents, m and n. The two scaling exponents, which are introduced into strain energy functions separated into deviatoric and volumetric components, are used to independently adjust volumetric and deviatoric elastic contributions, respectively. If $m = n = 0$, the extended model reduces to the original F–R model. In contrast, when the two exponents are adjusted based on experimental data, m spans a wide range of values depending on the elastomer, while n is a negative value that is almost independent of the elastomer. Consequently, the extended model successfully reproduces the effects of swelling on the Young's modulus and osmotic pressure of swollen elastomers, respectively. Further, under uniaxial tensile loading at equilibrium swelling, the extended model is able to predict strain softening, which is thus related with strain localization followed by swelling-induced rupture. This prediction is in good agreement with the tendency observed by experiments with natural rubbers [30]; swelling-induced rupture can occur when a small extension is applied in good solvents. This means that the two scaling exponents enable the extended model to obtain a special ability to predict swelling-induced rupture, resulting in elucidating the mechanism causing swelling-induced rupture of swollen elastomers.

Recently, Okumura and Mizutani [31] analyzed swelling-induced strain softening under equibiaxial and planar extensions using the two scaling exponents. They showed that under equibiaxial extension, the tensile stress in a lateral direction enables swelling-induced strain softening to occur in relatively poor solvents and accelerates the onset point. Under planar extension, a compressive stress in the constrained direction can occur in good solvents, preventing the elastomer from causing swelling-induced strain softening. The effects of two scaling exponents are fairly complicated under biaxial deformation. In addition, when a diffusion model is introduced to analyze mass

transport in the transient state, the evolution of the volume swelling ratio is affected not only by a diffusion coefficient but also by geometric and elastic contributions. The two scaling exponents also may have a considerable effect on mass transport in swollen elastomers. Thus, to accomplish a deeper understanding of this extended model with the two scaling exponents, it is necessary to investigate the effects on the biaxial deformation and mass transport of swollen elastomers.

In this study, we analyze the effects of the two scaling exponents on the biaxial deformation and mass transport of swollen elastomers. Section 2 presents the basic equations included in the extended model with the two scaling exponents and a diffusion model. In Section 3, mechanical responses under biaxial deformation are analyzed under stress and strain controls. Complicated behavior under strain control is interpreted by deriving and estimating Poisson's ratio at equilibrium free swelling. In Section 4, the effect of the two scaling exponents on mass transport is discussed by analyzing the swelling kinetics of a gel film constrained on a rigid substrate. Parametric studies are conducted in Sections 3 and 4. Finally, conclusions are presented in Section 5.

2. Basic equations

First, by extending the F–R model using the two scaling exponent [29], the free energy function is written as

$$W = \frac{E_{\mathrm{d}}}{6} J^{m}(I - 3J^{2/3}) + \frac{E_{\mathrm{d}}}{6} J^{n}(3J^{2/3} - 3 - a\log J) - \frac{kT}{\upsilon}\left\{\upsilon C \log\left(1 + \frac{1}{\upsilon C}\right) + \frac{\chi}{1+\upsilon C}\right\} \quad . \tag{1}$$

Here, the first and second terms on the right hand side are the elastic strain energy, and the third term is the mixing energy. Two scaling exponents, m and n, scale the deviatoric and volumetric parts of the elastic strain energy in the F–R model, respectively. Here, I and J are invariants, $I=F_{ij}F_{ij}$ and J =det $\boldsymbol{F}$ with the deformation gradient $F_{ij}=\partial x_i / \partial X_j$, which maps the reference frame X_j to the current frame x_i. The employment of the principal stretches $\lambda_i \ (i=1,2,3)$ leads to $I = \lambda_1^2 + \lambda_2^2 + \lambda_3^2$ and $J = \lambda_1 \lambda_2 \lambda_3$. In Eq.(1),

E_d is the Young's modulus of the undeformed, unswollen state at $\lambda_1 = \lambda_2 = \lambda_3 = 1$, and a is simply considered one of the fitting parameters. Moreover, C is the nominal concentration of solvent molecules, kT is the absolute temperature expressed as a thermal energy, υ is the volume per solvent molecule, and χ is the Flory–Huggins interaction parameter. It is noted that if $m=n=0$ and $a=2$, Eq.(1) is reduced to the original F–R model.

Assuming that the network of polymer and liquid solvent is incompressible, the volume of swollen elastomers is expressed as the sum of the volume of the dry network and that of the solvent [3]. The volume swelling ratio of swollen elastomers is equal to J, so that

$$J = 1 + \upsilon C. \tag{2}$$

When a Lagrange multiplier is used to impose the constraint of Eq.(2), Eq.(1) can be rewritten as

$$\begin{aligned} W = {} & \frac{E_d}{6} J^m (I - 3J^{2/3}) + \frac{E_d}{6} J^n (3J^{2/3} - 3 - a \log J) \\ & - \frac{kT}{\upsilon} \left\{ \upsilon C \log\left(1 + \frac{1}{\upsilon C}\right) + \frac{\chi}{1 + \upsilon C} \right\} + \Pi(1 + \upsilon C - J) \end{aligned}, \tag{3}$$

where Π is the Lagrange multiplier, and refers to the osmotic pressure in this study [5,29].

Eq.(3) gives the nominal stress in each direction of the principal stretches (i =1,2,3),

$$\begin{aligned} s_i = \frac{\partial W}{\partial \lambda_i} = {} & \frac{E_d}{3} \frac{J^m}{\lambda_i} \left\{ \lambda_i^2 - J^{2/3} + \frac{m}{2}(I - 3J^{2/3}) \right\} \\ & + \frac{E_d}{3} \frac{J^n}{\lambda_i} \left\{ J^{2/3} - \frac{a}{2} + \frac{n}{2}(3J^{2/3} - 3 - a \log J) \right\} - \Pi \frac{J}{\lambda_i} \end{aligned}, \tag{4}$$

while Eq.(4) is transformed into the true stress,

$$\begin{aligned} \sigma_i = \frac{s_i \lambda_i}{J} = {} & \frac{E_d}{3} J^{m-1} \left\{ \lambda_i^2 - J^{2/3} + \frac{m}{2}(I - 3J^{2/3}) \right\} \\ & + \frac{E_d}{3} J^{n-1} \left\{ J^{2/3} - \frac{a}{2} + \frac{n}{2}(3J^{2/3} - 3 - a \log J) \right\} - \Pi \end{aligned}. \tag{5}$$

When μ represents the chemical potential in swollen elastomers, Eqs.(2) and (3) give

$$\mu = \frac{\partial W}{\partial C} = kT \left\{ \log\left(\frac{J-1}{J}\right) + \frac{1}{J} + \frac{\chi}{J^2} \right\} + \Pi \upsilon. \tag{6}$$

The state of chemical equilibrium with respect to the external solvent is expressed as μ =0. Eq.(6) means that at equilibrium swelling (μ =0), the elastic component is balanced with the mixing component in swollen elastomers, so that Π refers to the osmotic pressure. In contrast, when $\mu = -\infty$, C =0 and $\lambda_i = J$ =1 in the underformed, unswollen state, so that this state is referred to as the underformed, unswollen state; equilibrium swelling can be reproduced by increasing μ from $-\infty$ to 0. Eqs.(4)–(6) are analyzed to investigate the effects of the two scaling exponents on the mechanical properties of swollen elastomers. Okumura et al. [29] demonstrated that this extended model satisfactorily reproduces the swelling effects on the Young's modulus and osmotic pressure of swollen elastomers at equilibrium swelling and also predicts swelling-induced strain softening.

Swollen elastomers need sufficient time to reach equilibrium swelling because swelling starts from the surface contacting the external solvent, and the gradient of the chemical potential is assumed to drive solvent migration. The transient state at time t can be analyzed by applying a diffusion model [12,15,17,32]. When a diffusion model is applied to solvent migration, the flux and concentration of solvent molecules can be written based on the reference and current flames, X_j and x_i, respectively. The nominal flux of solvent, J_k, is expressed as [32]

$$J_k = -M_{kl}\frac{\partial \mu}{\partial X_l}, \tag{7}$$

$$M_{kl} = \frac{D}{\upsilon kT}(J-1)F_{ki}^{-1}F_{li}^{-1}, \tag{8}$$

where D is a diffusion coefficient. Eq.(8) shows that the diffusion rate depends on M_{kl}, which includes D but is extended by the deformation gradient, F_{ij}, and J=det $\boldsymbol{F}$. Using Eqs.(7) and (8), the continuity equation for the nominal concentration of solvent molecules is written as

$$\frac{\partial C}{\partial t} = -\frac{\partial J_i}{\partial X_i} = \frac{\partial}{\partial X_i}\left(M_{il}\frac{\partial \mu}{\partial X_l}\right), \tag{9}$$

where μ consists of mixing and elastic contributions (see Eq.(6)) so that the transient state depends on the state of stresses via Π. This means that solvent migration is also

affected by the two scaling exponents.

The extended model has 8 material parameters, E_d, χ, υ, m, n, a, D, and kT, in Eqs.(1)–(9). When μ is normalized by kT (i.e, μ/kT), E_d is normalized as $E_d\,\upsilon/(3kT)$ (see Section 3). Further, t is normalized using D (see Section 4). In this case, the set of 5 material parameters, $E_d\,\upsilon/(3kT)$, χ, m, n, and a, have to be given before starting analysis. To eliminate redundancy, according to Okumura et al. [29], three representative sets of $E_d\,\upsilon/(3kT)$, m, n, and a, are primarily used in this study; first, $E_d\,\upsilon/(3kT)$=0.01, 0.05, and 0.1 are considered as representative values, and $E_d\,\upsilon/(3kT)$=0.01 is used with m = –0.3, n = –0.4, and a = –2, $E_d\,\upsilon/(3kT)$=0.05 with m = 0, n = –0.4, and a = –2, and $E_d\,\upsilon/(3kT)$=0.1 with m = 0.3, n = –0.4, and a = –4. Here, if the original F–R model is assumed, m = 0, n = 0, and a = 2 regardless of $E_d\,\upsilon/(3kT)$. In addition, χ is just parameterized in the range from 0 to 1. For $\chi < 0.5$, these values are regarded as good solvents, while for $\chi > 0.5$, poor solvents [3].

3. Biaxial responses

Fig. 1 shows schematic illustrations of biaxial tensile loading of an elastomer in a solvent. Biaxial tensile loading in the x_1 and x_2 directions are given while retaining equilibrium swelling (μ=0). The stress in the x_3 direction is always zero, i.e., $s_3 = \sigma_3 = 0$. Using $\sigma_1 = \sigma_1 - \sigma_3$, $\sigma_2 = \sigma_2 - \sigma_3$, Π vanishes from the true stress components of i =1 and 2 in Eq.(5), that is

$$\sigma_1 = \frac{E_d}{3} J^{m-1}(\lambda_1^2 - \lambda_3^2) = \frac{E_d}{3} J^{m-1}\left(\lambda_1^2 - \frac{J^2}{\lambda_1^2\lambda_2^2}\right), \tag{10}$$

$$\sigma_2 = \frac{E_d}{3} J^{m-1}(\lambda_2^2 - \lambda_3^2) = \frac{E_d}{3} J^{m-1}\left(\lambda_2^2 - \frac{J^2}{\lambda_1^2\lambda_2^2}\right). \tag{11}$$

Here, the relation $\lambda_3 = J\lambda_1^{-1}\lambda_2^{-1}$ is used to express them as a function of λ_1, λ_2, and J. When Eqs.(10) and (11) are transformed to the nominal stress (see Eq.(5)),

$$s_1 = \frac{E_d}{3} J^m\left(\lambda_1 - \frac{J^2}{\lambda_1^3\lambda_2^2}\right), \tag{12}$$

$$s_2 = \frac{E_d}{3} J^m \left(\lambda_2 - \frac{J^2}{\lambda_1^2 \lambda_2^3} \right). \tag{13}$$

Further, when σ_3 =0 is applied to the component of i =3 in Eq.(5), Π is also given as a function of λ_1, λ_2, and J. Eq.(6) leads to the following equation at equilibrium swelling (μ =0)

$$\begin{aligned} \frac{\mu}{kT} &= \left\{ \log\left(\frac{J-1}{J} \right) + \frac{1}{J} + \frac{\chi}{J^2} \right\} \\ &+ \frac{E_d \upsilon}{3kT} J^{m-1} \left\{ \frac{J^2}{\lambda_1^2 \lambda_2^2} - J^{2/3} + \frac{m}{2} \left(\lambda_1^2 + \lambda_2^2 + \frac{J^2}{\lambda_1^2 \lambda_2^2} - 3J^{2/3} \right) \right\}. \\ &+ \frac{E_d \upsilon}{3kT} J^{n-1} \left\{ J^{2/3} - \frac{a}{2} + \frac{n}{2} (3J^{2/3} - 3 - a \log J) \right\} = 0 \end{aligned} \tag{14}$$

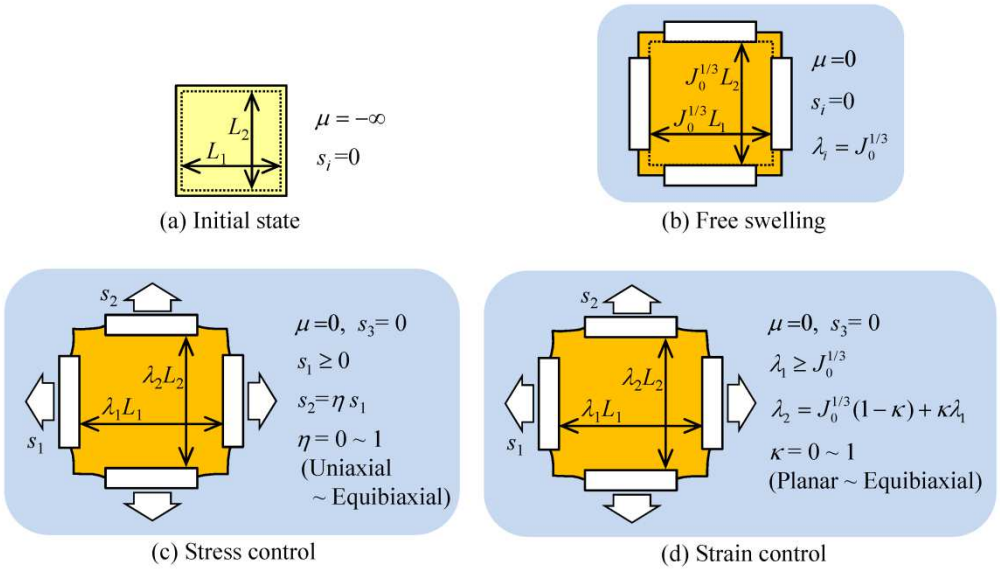

Fig. 1. Schematic illustration of biaxial tensile loading of an elastomer in a solvent; (a) initial state, (b) equilibrium free swelling, (c) stress control, and (d) strain control.

At equilibrium free swelling, $J = J_0$, $\lambda_1 = \lambda_2 = \lambda_3 = J_0^{1/3}$. In this case, Eqs.(12) and (13) show $s_1 = s_2 = 0$, while Eq.(14) represents

$$\left\{\log\left(\frac{J_0-1}{J_0}\right)+\frac{1}{J_0}+\frac{\chi}{J_0^2}\right\} + \frac{E_d\upsilon}{3kT}J_0^{n-1}\left\{J_0^{2/3}-\frac{a}{2}+\frac{n}{2}(3J_0^{2/3}-3-a\log J_0)\right\}=0 \quad (15)$$

where the second term in Eq.(14) vanishes in Eq.(15) because this term including m results from deviatoric deformation [29]. Eq.(15) is solved to obtain the volume swelling ratio J_0 at equilibrium free swelling. In the same manner, Eqs.(12)–(14) are solved to obtain the stress-stretch response under biaxial deformation at equilibrium swelling. Results under stress and strain controls are shown in Sections 3.1 and 3.2, respectively.

3.1. Under stress control

When s_1 and s_2 are given for Eqs.(12)–(14) (i.e., stress control), a set of λ_1, λ_2, and J is simultaneously solved. Analysis under stress control is performed with the biaxial stress ratio η;

$$s_2=\eta s_1, \quad (16)$$

where η =0 and 1 mean uniaxial tensile loading in the x_1 direction and equibiaxial tensile loading in the x_1 and x_2 directions. The biaxial stress ratio η is parameterized in the range from 0 to 1.

Fig.2 shows the nominal stress-stretch responses in the x_1 direction for η=0 (i.e., uniaxial), 0.5 (i.e., biaxial with a specific ratio) and 1 (i.e., equibiaxial). In the graphs, the combination of $E_d\upsilon/(3kT)$=0.01 and 0.1 with χ=0.2 and 0.6 is used to compare the responses of the extended model and the F–R model. First, the F–R model simply predicts a monotonic increase in s_1 as λ_1 increases and a relatively small influence of η regardless of the set of $E_d\upsilon/(3kT)$ and χ. Next, the extended model predicts considerably different responses depending on η as well as $E_d\upsilon/(3kT)$ and χ. Here, in Fig.2, the symbol □ represents the onset point at which strain softening starts. In the small case of $E_d\upsilon/(3kT)$=0.01, strain softening occurs with χ=0.2 and 0.6. The critical stresses normalized by E_d are in the wide range from s_c/E_d =0.1~0.6, and the critical

stretches are also in the wide range from λ_c=2.5~10 (Fig.2a,b). In contrast, when the large case of $E_d\upsilon/(3kT)$=0.1 is focused on, χ=0.6 predicts a monotonic increase in s_1 without inducing strain softening (Fig.2c), but χ=0.2 predicts the onset of strain softening, especially at small values of λ_c (Fig.2d). As reported in Okumura et al. [29], this tendency is consistent with Gee's experiments with natural rubbers [30], stating that "with good swelling agents, only very small extensions can be applied without breaking the specimen." Fig.2 shows that the onset points of strain softening are considerably affected not only by the interaction parameter χ but also by the biaxial stress ratio η.

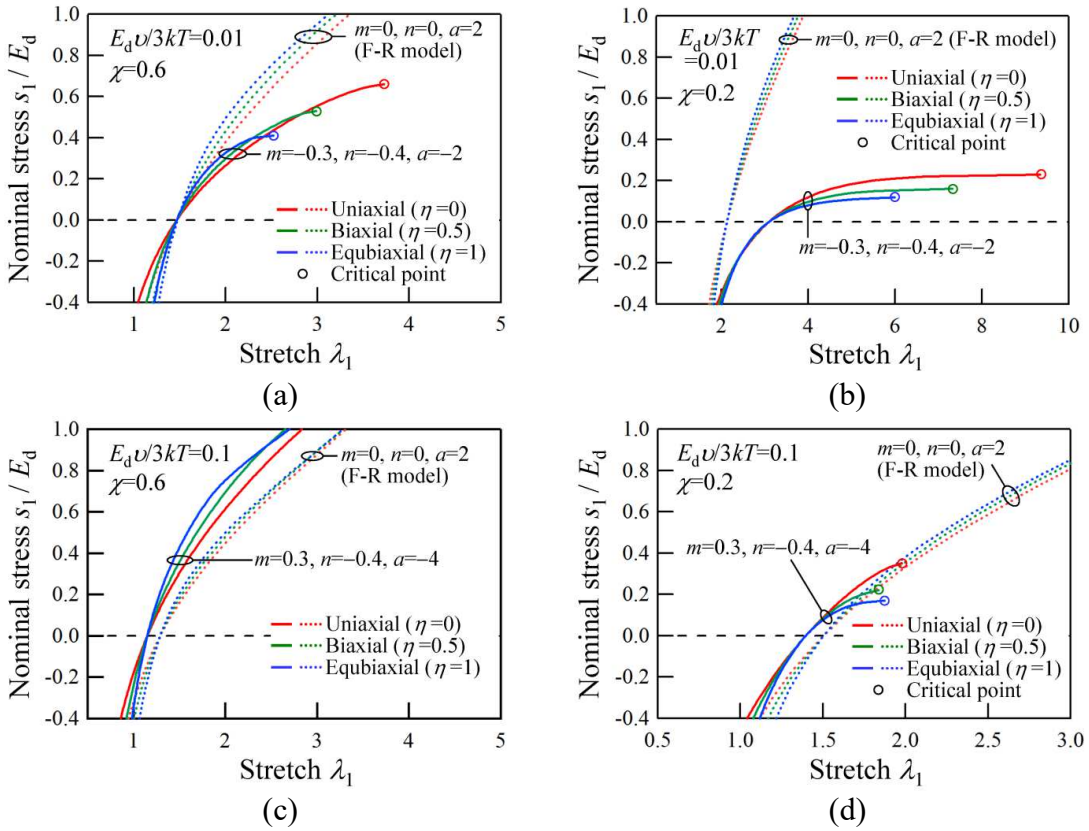

Fig. 2. Stress-stretch responses at equilibrium swelling under uniaxial loading ($s_2 = 0$), biaxial loading ($s_2 = 0.5\ s_1$) and equibiaxial loading ($s_2 = s_1$); (a) $E_d\upsilon/(3kT) = 0.01$ and χ=0.6, (b) $E_d\upsilon/(3kT) = 0.01$ and χ=0.2, (c) $E_d\upsilon/(3kT) = 0.1$ and χ=0.6, and (d) $E_d\upsilon/(3kT) = 0.1$ and χ=0.2.

To make clear the effect of biaxial deformation (i.e., the effect of η in this section), on the onset of strain softening, Fig.3 shows the critical stress as a function of the interaction parameter χ for $E_d\upsilon/(3kT)$=0.01 (Fig.3a) and 0.1 (Fig.3b). It is found that the biaxial stress ratio (η=0, 0.5 and 1) affects critical stresses, but the overall profiles

depend on the set of $E_d\ \upsilon/(3kT)$, m, n, and a. The increase in the tensile stress in the lateral direction (i.e., the increase in η) enables strain softening to occur not only in the earlier stage of deformation but also in relatively poor solvents (cf.[31]). This quantitative relation seems to be nonlinear as a function of η (Fig.3). When s_1 and s_2 at the critical point are plotted as a function of η in the range from 0 to 1, the critical stress surface is obtained (Fig.4). In the case of χ =0.4 for the parameter set including $E_d\ \upsilon/(3kT)$=0.1 (Fig.4b), strain softening does not occur under uniaxial extension but does occur under biaxial loading, and the stress surface becomes nonconvex. This feature can be understood also from Figs.3b.

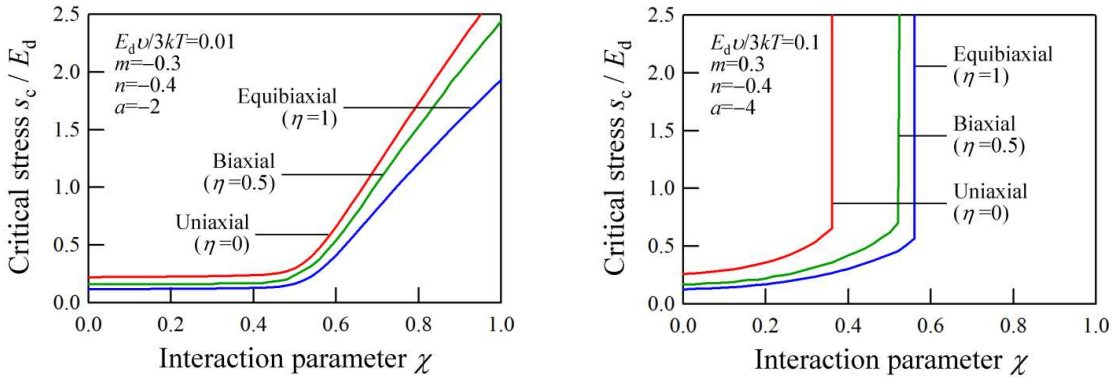

Fig. 3. Critical stress in the x_1 direction, s_c, at which strain softening begins as a function of χ ; (a) $E_d\upsilon/(3kT)$ = 0.01 and (b) $E_d\upsilon/(3kT)$ = 0.1.

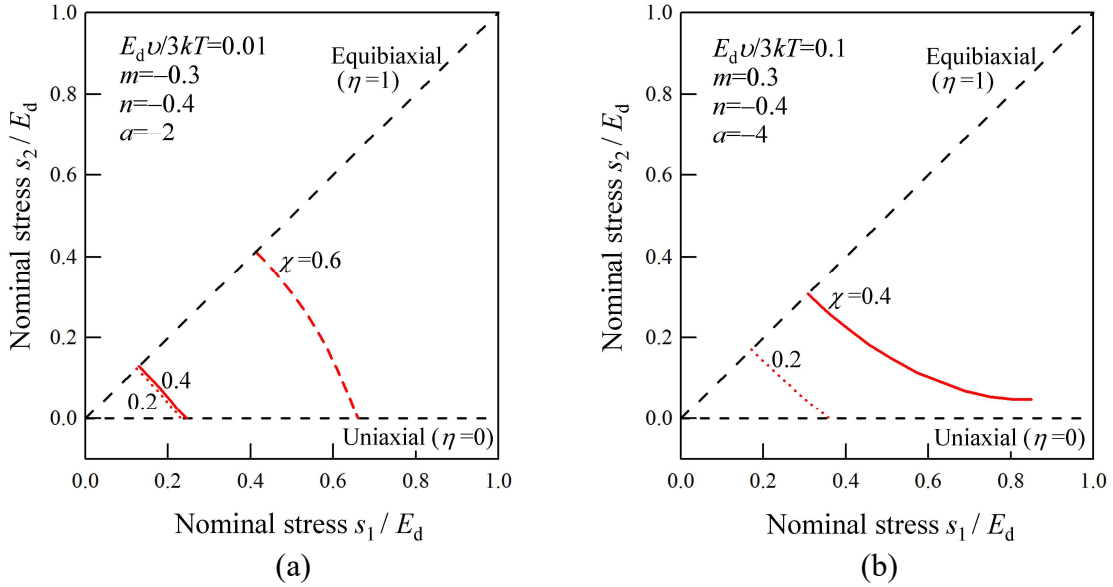

Fig. 4. Critical stress surface in s_1 and s_2 predicted by biaxial tensile loading; (a) $E_d\upsilon/(3kT)$ = 0.01 and (b) $E_d\upsilon/(3kT)$ = 0.1.

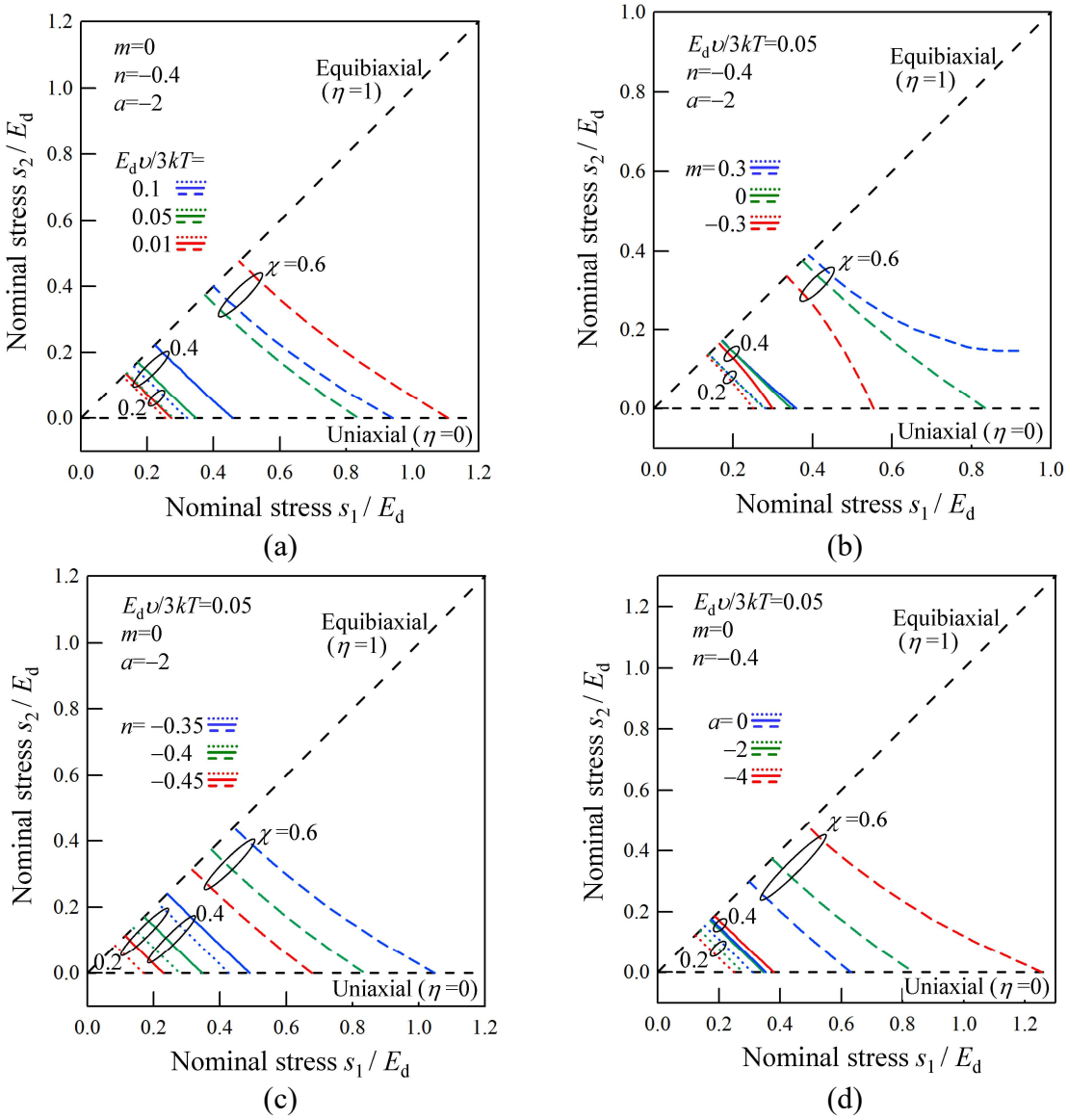

Fig. 5. Effects on critical stress surface in s_1 and s_2 obtained by parametrizing (a) $E_d\upsilon/(3kT)$ = 0.01, 0.05, and 0.1, (b) m = –0.3, 0, and 0.3, (c) n = –0.6, –0.4, and –0.2 and (d) a = –4, –2, and 0.

Fig.5 depicts the critical stress surface under biaxial deformation obtained by parametrizing one of $E_d\ \upsilon\ /(3kT)$, m, n, and a, when the parameter set of $E_d\ \upsilon\ /(3kT)$=0.05, m = 0, n = –0.4 and a = –2 is considered as a base elastomer. Although in the case of uniaxial tensile loading, the parametric studies were conducted in Okumura et al. [29], the effect of the tensile stress in the lateral direction can be investigated in Fig.5. First, the contributions of these parameters become larger as the solvent becomes poorer. However, the scaling factor n is dominant both in poor and good solvents

(Fig.5c). Next, the contributions of $E_d\ \upsilon\ /(3kT)$, n, and a do not yield different tendencies in the presence of η (Fig.5a,c,d), while the effect of m changes as η increases from 1 to 0 (Fig.5b). It is noted that if m increases from 0 to a positive value, this increase acts to prevent strain softening from occurring under uniaxial tensile loading. Thus, if m decreases from 0 to a negative value, this decrease acts to accelerate strain softening under uniaxial tensile loading. The different tendency in Fig.4a,b is caused by m =–0.3 or 0.3 in the parameter sets including $E_d\ \upsilon\ /(3kT)$=0.01 or 0.1, respectively. Fig.5 shows that the scaling factor m can cause the difference between uniaxial and biaxial extensions (cf. $E_d\ \upsilon\ /(3kT)$, n, and a) and that this effect appears strongly under uniaxial loading because m is the scaling factor introduced into the deviatoric component of the elastic strain energy and n and a are only included in the volumetric component.

3.2. Under strain control

When λ_1 and λ_2 are given for Eqs.(12)–(14) (i.e., strain control), a set of s_1, s_2, and J is solved; Eq.(14) is first solved to obtain J, and then Eqs.(12) and (13) give s_1 and s_2, respectively. Analysis under strain control is performed with the biaxial strain ratio κ. When strains ε_1 and ε_2 are connected with λ_1 and λ_2 as follows

$$\begin{cases} \lambda_1 = J_0^{1/3}(1+\varepsilon_1) \\ \lambda_2 = J_0^{1/3}(1+\varepsilon_2) \end{cases}, \tag{17}$$

the biaxial strain ratio κ is defined as

$$\varepsilon_2 = \kappa\varepsilon_1, \tag{18}$$

where κ =0 expresses planar extension in the x_1 direction with the constraint in the x_2 direction (i.e., $\lambda_2 = J_0^{1/3}$ is constrained), while κ =1 expresses equibiaxial tensile loading, which is equivalent to η =1 under stress control. Eqs.(17) and (18) allow λ_2 to be an explicit function of λ_1 and κ, that is,

$$\lambda_2 = J_0^{1/3}(1-\kappa) + \kappa\lambda_1. \tag{19}$$

The biaxial strain ratio κ is also parameterized in the range from 0 to 1. In this case, a biaxial extension is imposed to the elastomer because as λ_1 increases, ε_1 and ε_2 increase from zero to positive values.

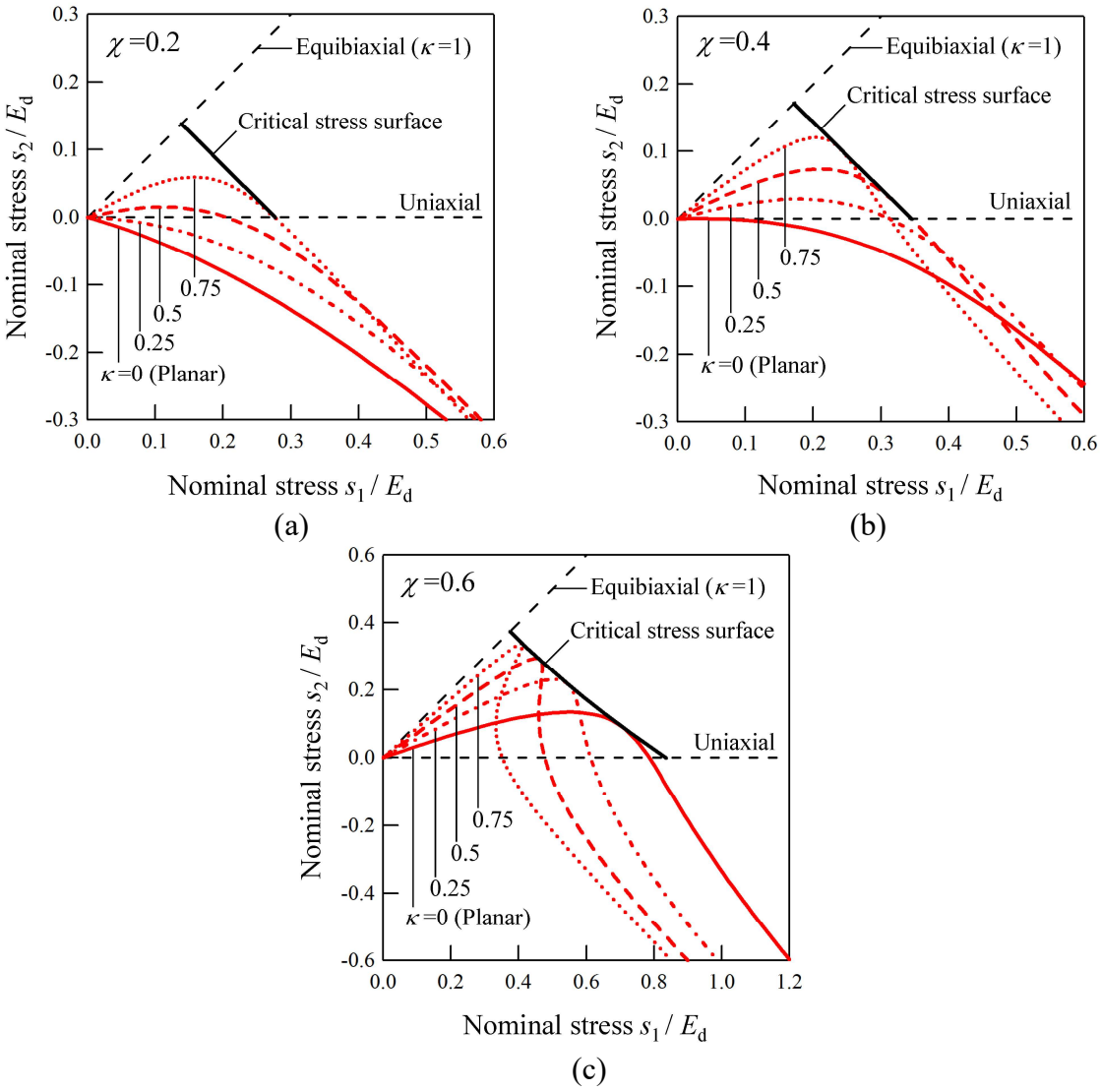

Fig. 6. Comparison of stress trajectory under strain control for $E_d\upsilon/(3kT) = 0.05$, $m = 0$, $n = -0.4$, and $a = -2$; (a) $\chi = 0.2$, (b) $\chi = 0.4$, and (c) $\chi = 0.6$.

Fig.6 shows the stress trajectory under biaxial loading when the biaxial strain ratio is controlled as κ=0, 0.25, 0.5, and 0.75. The result of κ=1 is equivalent to η=1 under stress control because both cases express equibiaxial loading. The parameter set of a base elastomer (i.e., $E_d\ \upsilon/(3kT)$=0.05, $m = 0$, $n = -0.4$, and $a = -2$) is used for χ=0.2, 0.4, and 0.6. In Fig.6, the critical stress surface, which was analyzed under stress control

in Section 3.1, is plotted to understand the responses under strain control. When a poor solvent is considered (Fig.6c), biaxial extension caused by ε_1 and ε_2 yields a biaxial tensile state of $s_1 > 0$ and $s_2 > 0$. The biaxial tensile state arrives at the critical stress surface early or late, so that strain softening can occur under strain control. After the onset of strain softening, the responses become complicated to preserve the value of κ. In contrast, the responses in good solvents (Fig.6a,b) do not yield the same behavior as in poor solvents (Fig.6c). In Fig.6a,b, strain softening does not occur clearly for χ =0.2 and 0.4, excluding the combination of κ =0.5 and 0.75, and χ =0.4. This unexpected behavior is explained by considering the change in the stress in the lateral direction. In particular, for κ =0 and 0.25 for χ =0.2 and κ =0 for χ =0.4, the stress in the lateral direction does not take a positive value but starts to take a negative value at an early stage of biaxial deformation. As shown in Section 3.1, the tensile stress in the lateral direction accelerates the onset of strain softening, so that the negative stress is expected to prevent strain softening from occurring. The results show that under strain control, a compressive stress can be generated in the lateral direction, which has the tendency to appear in good solvents and in the case of small κ. Incidentally, this behavior was first discussed by analysis under planar extension [31].

In general, biaxial extension under strain control ($\varepsilon_1 > 0$ and $\varepsilon_2 > 0$) causes a biaxial tensile stress state when Poisson's ratio is assumed to be positive. Thus, Fig.6 implies that the extended model can predict that swollen elastomers at equilibrium free swelling have a negative Poisson's ratio. Bouklus and Huang [32] derived a closed form expression of Poisson's ratio, which are derived from the F–R model. Further, Okumura et al. [29] successfully extended it in the case of an extended model with two scaling exponents. According to [29], when Eqs.(5) and (6) are linearized under uniaxial loading without a change in the chemical potential, Poisson's ratio, ν, can be expressed as the closed form expression

$$\nu = \frac{1}{2} - \frac{1}{2}\frac{E_\mathrm{d}\upsilon}{3kT} J_0^{m-1/3} \left\{ \frac{1}{J_0 - 1} - \frac{1}{J_0} - \frac{2\chi}{J_0^2} + \frac{E_\mathrm{d}\upsilon}{3kT} X \right\}^{-1}, \tag{20}$$

$$X = \frac{1}{3} J_0^{m-1/3} + J_0^{n-1} \left\{ \frac{(3n+2)(3n-1)}{6} J_0^{2/3} - \frac{2n-1}{2} a - \frac{n(n-1)}{2} (3 + a \log J_0) \right\}. \quad (21)$$

If m =0, n =0, and a =2, Eqs.(20) and (21) reduce to that derived by Bouklus and Huang [32]. It is noted that Eqs.(20) and (21) are the closed form expression to estimate Poisson's ratio with a volume swelling ratio J_0. In this study, the volume swelling ratio at equilibrium free swelling is denoted as J_0, so that J_0 is analyzed by solving Eq.(15).

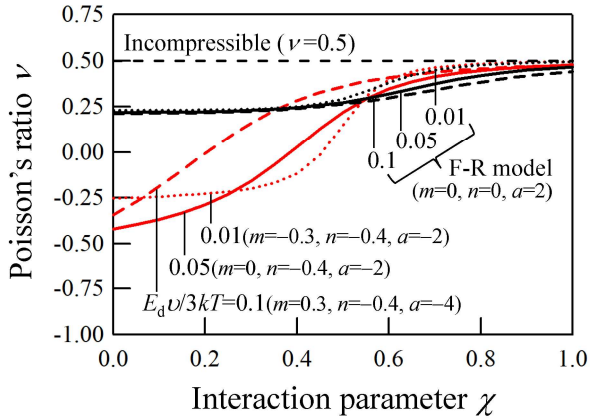

Fig. 7. Poisson's ratio at equilibrium free swelling as a function of interaction parameter χ for $E_d\upsilon/(3kT)$ = 0.01, 0.05, and 0.1.

Fig.7 shows Poisson's ratio as a function of the interaction parameter χ for the three representative sets of $E_d\ \upsilon/(3kT)$, m, n, and a (see Section 2). If swollen elastomers are incompressible, ν=0.5, but they are compressible depending on the increase in J during swelling when the change in the chemical potential in swollen elastomers is not allowed. Thus, as χ increases more than about approximately 1 (i.e., poor solvents), Poisson's ratio approaches 0.5 regardless of $E_d\ \upsilon/(3kT)$, m, n, and a. As χ decreases from 1, Poisson's ratio is affected by the increase in J; Poisson's ratio takes a smaller value compared with 0.5. When good solvents are assumed in the F–R model (i.e., χ <0.5), Poisson's ratio is approximately 0.25. This value is not sensitive to $E_d\ \upsilon/(3kT)$ in good solvents. In contrast, in the extended model, the profiles depend considerably on the set of parameters. In good solvents, the extended model predicts the negativity of Poisson's ratio. In the case of a base elastomer (i.e., $E_d\ \upsilon/(3kT)$=0.05, m = 0, n = –0.4, and a = –2), Poisson's ratio is smaller than zero as χ decreases from approximately 0.4. This feature

causes a compressive stress in the lateral direction under biaxial deformation (see Fig.6).

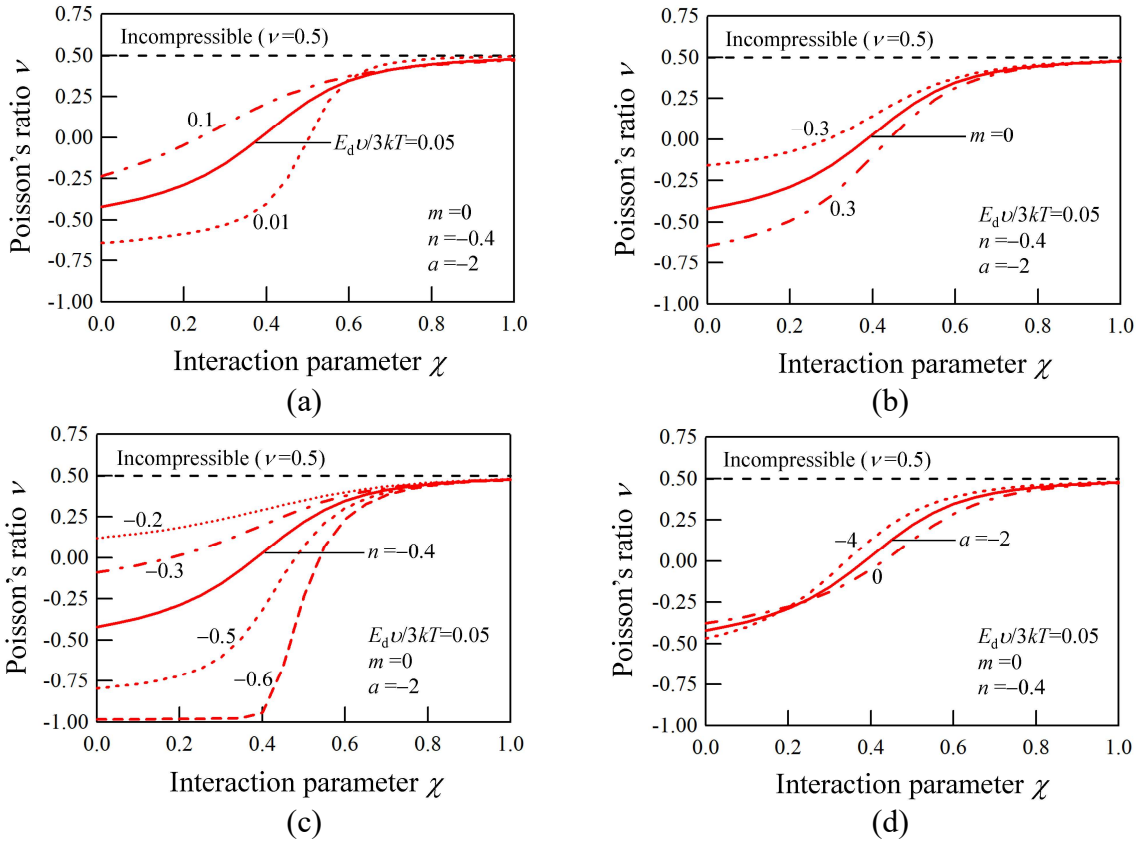

Fig. 8. Effects on Poisson's ratio at equilibrium free swelling obtained by parametrizing (a) $E_d\upsilon/(3kT)$ = 0.01, 0.05, and 0.1, (b) m = –0.3, 0, and 0.3, (c) n = –0.6, –0.5, –0.4, –0.3, and –0.2 and (d) a = –4, –2, and 0.

Fig.8 depicts the dependence of Poisson's ratio on χ obtained by parametrizing one of $E_d\ \upsilon/(3kT)$, m, n, and a. Although the F–R model predicts almost no dependence of $E_d\ \upsilon/(3kT)$ in good solvents (see Fig.7), the extended model shows a considerable dependence of m and n as well as $E_d\ \upsilon/(3kT)$, while a has a small effect (Fig.8d). As $E_d\ \upsilon/(3kT)$ decreases with n =–0.4 (Fig.8a), Poisson's ratio decreases from a positive value to a negative value. In the same manner, the changes in m and n cause dramatic changes in Poisson's ratio. Incidentally, it may be interesting to discuss the reason that Poisson's ratio tends to be saturated to –1 if n is assumed to be smaller than approximately –0.6 in good solvents (Fig.8c). In this extreme case, when a stretch is imposed in a direction, this stretch is provided by the change in J, (i.e., $\lambda = J^{1/3}$), so that the stretches in other directions are also identical, i.e., $\nu = -1$. As a result of the combination of $E_d\ \upsilon/(3kT)$, m,

n, and a, the negativity of Poisson's ratio can appear when the extended model is assumed in good solvents. The complicated responses under strain control can be interpreted by considering this feature.

4. Transient responses of constrained gel layer

To investigate the effect of two scaling exponents on mass transport, the swelling kinetics of a gel layer constrained on a rigid substrate is analyzed. Fig.9 shows schematic illustrations of an elastomer layer constrained on a rigid substrate at the bottom face ($X_3 = 0$) and exposed to a solvent on the top face ($X_3 = H$). When the top face is assumed to remain flat during swelling, the gradient of the chemical potential appears only in the X_3 direction (i.e., $\partial\mu/\partial X_1 = \partial\mu/\partial X_2 = 0$ and $\partial\mu/\partial X_3 \neq 0$). The lateral dimensions are fixed by the substrate constraint so that deformation is allowed only in the X_3 direction. This constraint results in increasing the compressive stresses in the X_1 and X_2 directions during swelling, while the stress in the X_3 direction always remains zero (s_3=0). These assumptions mean that surface instability is not considered in the present study.

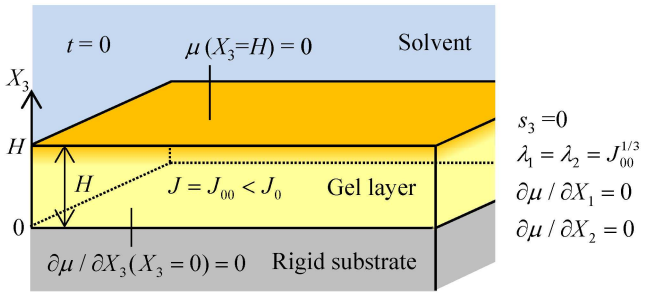

Fig. 9. Schematic illustration and boundary conditions of a gel layer constrained on a rigid substrate at the bottom face ($X_3 = 0$) and exposed to a solvent on the top face ($X_3 = H$).

When X_1, X_2, and X_3 are assigned to the principal directions of i =1,2,3, respectively, the deformation gradient is explicitly expressed as

$$F_{kl} = \begin{pmatrix} \lambda_1 & 0 & 0 \\ 0 & \lambda_2 & 0 \\ 0 & 0 & \lambda_3 \end{pmatrix} = \begin{pmatrix} J_{00}^{1/3} & 0 & 0 \\ 0 & J_{00}^{1/3} & 0 \\ 0 & 0 & JJ_{00}^{-2/3} \end{pmatrix}, \tag{22}$$

where J_{00} is the initial value of the volume swelling ratio in the reference state (t =0), and J is the current value and is a function of t. The reference state is given as J_{00} under free swelling, i.e., $\lambda_1 = \lambda_2 = \lambda_3 = J_{00}^{1/3}$ with s_i =0 but μ<0 so that $1 < J_{00} < J_0$ (cf. Section 3). In the current state, $J = \lambda_1\,\lambda_2\,\lambda_3$ results in $\lambda_3 = JJ_{00}^{-2/3}$. Using Eq.(22), Eq.(8) gives

$$M_{33} = \frac{D}{\upsilon kT}\frac{J_{00}^{4/3}(J-1)}{J^2}, \tag{23}$$

where M_{11} and M_{22} can also be derived with nonzero values, but they are not effective in this analysis because $\partial\mu/\partial X_1 = \partial\mu/\partial X_2 = 0$ (see Eq.(7)). Further, Eq.(14) gives

$$\begin{aligned}\frac{\mu}{kT} &= \left\{\log\left(\frac{J-1}{J}\right)+\frac{1}{J}+\frac{\chi}{J^2}\right\}\\ &+\frac{E_\mathrm{d}\upsilon}{3kT}J^{m-1}\left\{\frac{J^2}{J_{00}^{4/3}}-J^{2/3}+\frac{m}{2}\left(2J_{00}^{2/3}+\frac{J^2}{J_{00}^{4/3}}-3J^{2/3}\right)\right\},\\ &+\frac{E_\mathrm{d}\upsilon}{3kT}J^{n-1}\left\{J^{2/3}-\frac{a}{2}+\frac{n}{2}(3J^{2/3}-3-a\log J)\right\}\end{aligned} \tag{24}$$

resulting in

$$\frac{1}{kT}\frac{\partial\mu}{\partial X_3} = \left\{\frac{1}{J^2(J-1)}-\frac{2\chi}{J^3}+\frac{E_\mathrm{d}\upsilon}{3kT}(Y+Z)\right\}\frac{\partial J}{\partial X_3}, \tag{25}$$

$$Y = J^{m-2}\left\{\frac{(m+1)(m+2)}{2}\frac{J^2}{J_{00}^{4/3}}-\frac{(3m+2)(3m-1)}{6}J^{2/3}+m(m-1)J_{00}^{2/3}\right\}, \tag{26}$$

$$Z = J^{n-2}\left\{\frac{(3n+2)(3n-1)}{6}J^{2/3}-\frac{2n-1}{2}a-\frac{n(n-1)}{2}(3+a\log J)\right\}. \tag{27}$$

Eqs.(2),(9),(23),(25)–(27) give the evolution equation for the volume swelling ratio as a function of t and X_3. When t and X_3 are normalized by H^2/D and H, respectively, the evolution equation is expressed as

$$\frac{\partial J}{\partial \bar{t}} = \frac{\partial}{\partial \bar{X}}\left(\Lambda\frac{\partial J}{\partial \bar{X}}\right), \tag{28}$$

$$\Lambda = \frac{J_{00}^{4/3}(J-1)}{J^2}\left\{\frac{1}{J^2(J-1)}-\frac{2\chi}{J^3}+\frac{E_\mathrm{d}\upsilon}{3kT}(Y+Z)\right\}, \tag{29}$$

where $\bar{t} = tD/H^2 \geq 0$, $\bar{X} = X_3/H$ with $0 \leq \bar{X} \leq 1$. Here, Λ is defined as a mobility factor in the present study. This factor is a function of J and depends on J_{00}, χ, E_d υ

/(3kT), m, n, and a. In the kinetic responses of this problem, the effects of the two scaling exponents are introduced in Eq.(29) via two terms of Eqs.(26) and (27).

Eq.(28) needs initial and boundary conditions (Fig.9). At t =0, J =J_{00} everywhere except for the top face ($\bar{X}=1$). At $\bar{X}=1$, μ =0 results in J =J_0 at any time. Here, J_0 is calculated by solving Eq.(24) with μ =0. At the bottom face ($\bar{X}=0$), J_3 =0 results in $\partial J / \partial X_3 = 0$ at any time. Eq.(28) is finally solved by a finite differential method [32]. It is noted here that the evolution equation was solved in [32] as a function of the stretch in the thickness direction, while in the present study, the volume swelling ratio is solved using Eq.(29), but the translation from J to λ_3 is easy because $\lambda_3 = JJ_{00}^{-2/3}$ (Eq.(22)).

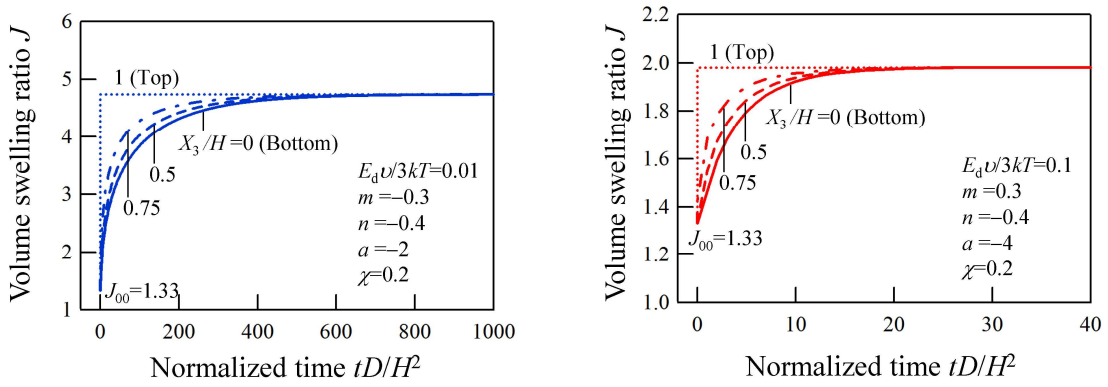

Fig. 10. Evolution of volume swelling ratio, J, as a function of normalized time, tD/H^2, for X_3/H =0, 0.5, 0.75, and 1 with χ = 0.2 and J_{00} = 1.33; (a) $E_d\Omega/(3kT)$ = 0.01 and (b) $E_d\Omega/(3kT)$ = 0.1.

Fig.10 shows the results with the volume swelling ratio, J, as a function of the normalized time, tD/H^2, for X_3/H=0, 0.5, 0.75, and 1. Fig.10 is obtained using J_{00}=1.33 and χ =0.2. As X_3 decreases from the top face to the bottom face, the increase in J becomes slow because of the delay of solvent migration. Fig.10a,b show the difference between the two parameter sets. In Fig.10a, the parameter set allows a larger volume swelling ratio ($J\approx5$) compared with that in Fig.10b ($J\approx2$). This feature is directly related to the difference in the time at which the volume swelling ratio at the bottom face approaches equilibrium swelling. Fig.10 simply shows that the time needed to obtain equilibrium swelling everywhere depends on the increasing amount of the

volume swelling ratio from J_{00} to J_0. It is not clear if the two scaling exponents play an important role in causing the remarkable difference in the transient state.

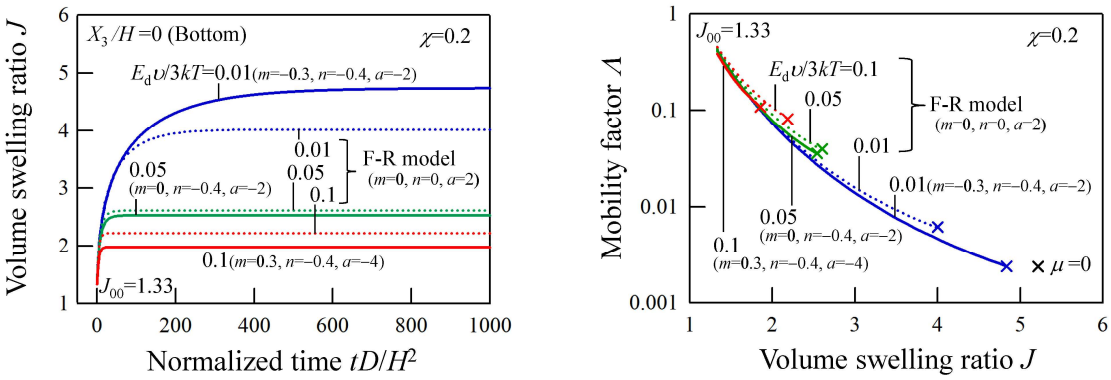

Fig. 11. Comparison of evolution of mass transport; (a) volume swelling ratio, J, at the bottom face (X_3/H=0), as a function of normalized time, tD/H^2, and (b) mobility factor, Λ (Eq.(29)), as a function of volume swelling ratio, J.

When the volume swelling ratio at the bottom face is focused on, Fig.11 shows the results obtained by the F–R and extended models. Fig.11a shows the dependence of the volume swelling ratio at equilibrium swelling on $E_d\,\upsilon/(3kT)$, m, n, and a, while Fig.11b shows the dependence of the mobility factor Λ on $E_d\,\upsilon/(3kT)$, m, n, and a. This graph demonstrates that the mobility factor predicted by the extended model is slightly smaller than that predicted by the F–R model when $E_d\,\upsilon/(3kT)$ is identical (Fig.11b). These results show that the extended model predicts a slightly slow diffusion process when m, n, and a are adjusted by experiments [29]. Fig.12 depicts the dependence of Λ on J obtained by parametrizing one of $E_d\,\upsilon/(3kT)$, m, n, and a. Unexpectedly, the effect of n as well as $E_d\,\upsilon/(3kT)$ is negligible in this profile, although they affect the volume swelling ratio at equilibrium swelling (Fig.12a,c). Fig.12b,d show that the mobility factor tends to decrease as m and a decrease to a negative value. This tendency yields the difference between the F–R and extended models in Fig.11. However, these differences also may be negligible. The results obtained in this section demonstrate that the extended model modifies the mobility factor Λ using the two scaling exponents, but the contributions to the swelling kinetics are not considerably large.

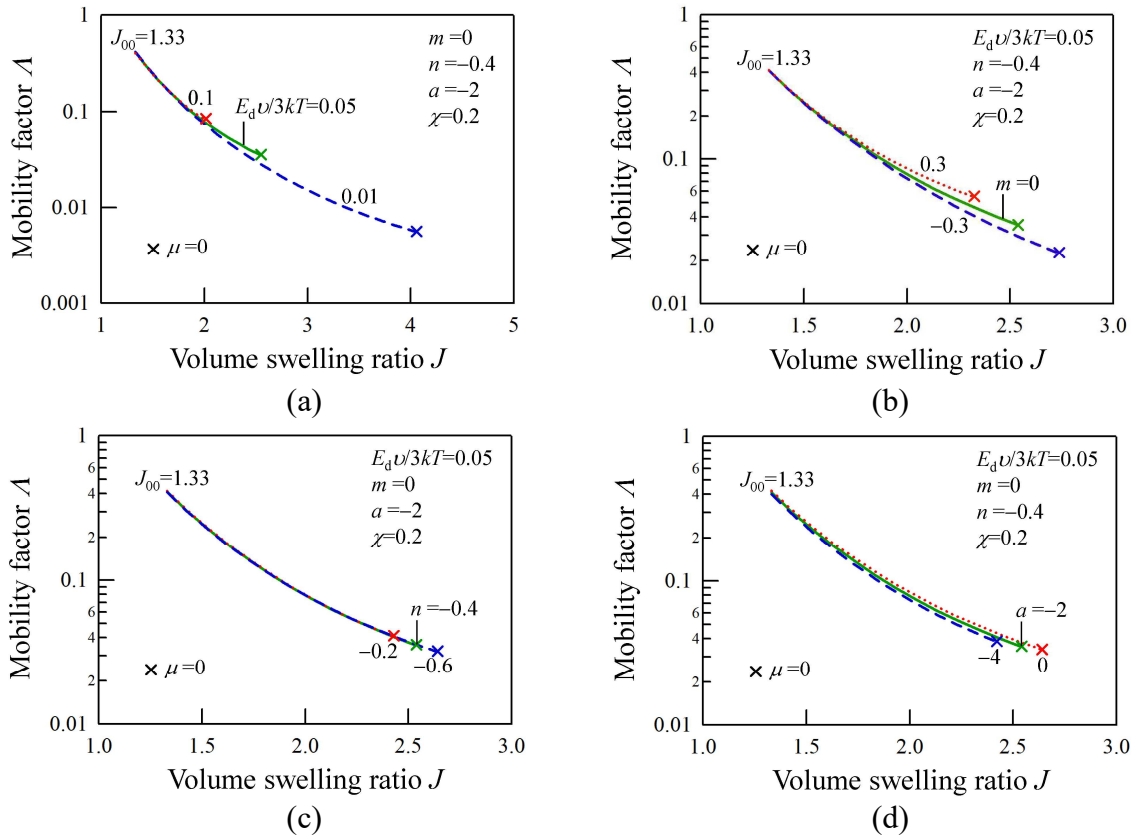

Fig. 12. Effects on mobility factor, Λ (Eq.(29)), with $\chi = 0.2$ and $J_{00} = 1.33$, obtained by parametrizing (a) $E_d\upsilon/(3kT) = 0.01$, 0.05, and 0.1, (b) $m = -0.3$, 0, and 0.3, (c) $n = -0.6$, -0.4, and -0.2 and (d) $a = -4$, -2, and 0.

5. Concluding remarks

In the present study, the effects of two scaling exponents on the biaxial deformation and mass transport of swollen elastomers were investigated. The two scaling exponents are included in an extended version of the Flory–Rehner model [29]. When biaxial tensile loading was given under stress control, the increase in the biaxial stress ratio enabled strain softening to occur not only in the earlier stage of deformation, but also in relatively poor solvents. In contrast, under strain control, strain softening was prevented by a compressive stress in the lateral direction, which can be generated in good solvents and in the case of small biaxial strain ratio (e.g., planar extension). This complicated behavior was interpreted by considering that Poisson's ratio at equilibrium free swelling can take negative values depending on the two scaling exponents. Further, in the analysis of the swelling kinetics of a constrained gel layer, the two scaling exponents act via the mobility factor of Eq.(29). Although the two scaling exponents had a remarkable

influence on the volume swelling ratio at equilibrium swelling, their effects on solvent migration during swelling were not as dramatic. However, the mobility factor has a tendency to decrease to a greater or lesser extent as m and a decrease to a negative value.

In the present study, the neo-Hookean solid model extended by two scaling exponents [29] was used to investigate the effects of the biaxial deformation and mass transport of swollen elastomers. The swelling effects were adjusted well using the two scaling exponents, but this extended model may not have the ability to predict the mechanical responses at large strain and/or under biaxial deformation. It will be possible to extend more advanced solid models using the two scaling exponents. To perform this extension, more elaborate studies of the swelling effects at large strain under biaxial deformation should be conducted. The dependence of the swelling kinetics of elastomers on internal stresses should be further investigated. These future studies will achieve more comprehensive understanding and modeling of swollen elastomers in static and transient states.

Acknowledgments

This research was supported by the Japan Society for the Promotion of Science (JSPS) under a Grant-in-Aid for Scientific Research (B) (No.16H04234).

References

[1] Flory PJ, Rehner J, Statistical mechanics of cross-linked polymer networks II. Swelling. J Chem Phys 1943;11:521–6.

[2] Flory PJ, Principles of Polymer Chemistry, 1953, Cornell University Press: Ithaca, NY.

[3] Treloar LRG, The Physics of Rubber Elasticity, 3rd ed, 1975, Clarendon Press: Oxford.

[4] Hong W, Liu ZS, Suo Z, Inhomogeneous swelling of a gel in equilibrium with a solvent and mechanical load. Int J Solids Struct 2009;46:3282–9.

[5] Kang MK, Huang R, A variational approach and finite element implementation for swelling of polymeric hydrogels under geometric constraints. J Appl Mech 2010;77:061004.

[6] Kang MK, Huang R, Swell-induced surface instability of confined hydrogel layers on substrates. J Mech Phys Solids 2010;58:1582–98.

[7] Wu Z, Bouklas N, Huang R, Swell-induced surface instability of hydrogel layers with material properties varying in thickness direction. Int J Solids Struct 2013;50:578–87.

[8] Ding ZW, Liu ZS, Hu JY, Swaddiwudhipong S, Yang ZZ, Inhomogeneous large deformation study of temperature-sensitive hydrogel. Int J Solids Struct 2013;50;2610–9.

[9] Okumura D, Kuwayama T, Ohno N, Effect of geometrical imperfections on swelling-induced buckling patterns in gel films with a square lattice of holes. Int J Solids Struct 2014;51:154–63.

[10] Okumura D, Inagaki T, Ohno N, Effect of prestrains on swelling-induced buckling patterns in gel films with a square lattice of holes. Int J Solids Struct 2015;58:288–300.

[11] Okumura D, Sasaki A, Ohno N, Swelling-induced buckling patterns in gel films with a square lattice of holes subjected to in-plane uniaxial and biaxial pretensions. Adv Structured Mater 2015; 64:319–34.

[12] Hong W, Zhao XH, Zhou JX, Suo Z, A theory of coupled diffusion and large deformation in polymeric gels. J Mech Phys Solids 2008;56:1779–93.

[13] Chester SA, Anand L, A coupled theory of fluid permeation and large deformations for elastomeric materials. J Mech Phys Solids 2010;58:1879–906.

[14] Duda FP, Souza AC, Fried E, A theory for species migration in a finitely strained solid with application to polymer network swelling. J Mech Phys Solids 2010;58:515–29.

[15] Toh W, Liu Z, Ng TY, Hong W, Inhomogeneous large deformation kinetics of polymeric gels. Int J Appl Mech 2013;5:1350001.

[16] Wilmers J, Bargmann S, A continuum mechanical model for the description of solvent induced swelling in polymeric glasses: Thermomechanics coupled with diffusion. Euro J Mech A 2015;53:10–8.

[17] Bouklas N, Landis CM, Huang R, A nonlinear, transient finite element method for coupled solvent diffusion and large deformation of hydrogels. J Mech Phys Solids 2015;79:21–43.

[18] Chester SA, Di Leo CV, Anand L, A finite element implementation of a coupled diffusion-deformation theory for elastomeric gels. Int J Solids Struct 2015;52:1–18.

[19] Han WH, Horkay F, McKenna GB, Mechanical and swelling behaviors of rubber: a comparison of some molecular models with experiment. Math Mech Solids 1999;4:139–67.

[20] Arruda EM, Boyce MC, A three-dimensional model for the large stretch behavior of rubber elastic materials. J Mech Phys Solids 1993;41:389–412.

[21] Boyce MC, Arruda EM, Swelling and mechanical stretching of elastomeric materials. Math Mech Solids 2001;6:641–59.

[22] McKenna GB, Flynn KM, Chen Y, Experiments on the elasticity of dry and swollen networks: implications for the Frenkel-Flory-Rehner hypothesis. Macromolecules 1989;22:4507–12.

[23] Bitoh Y, Akuzawa N, Urayama K, Takigawa T, Strain energy function of swollen polybutadiene elastomers studied by general biaxial strain testing. J Polymer Sci 2010;B48:721–8.

[24] Flory PJ, Erman B, Theory of elasticity of polymer networks 3. Macromolecules 1982;15:800–6.

[25] Drozdov AD, Christiansen JdeC, Constitutive equations in finite elasticity of

swollen elastomers. Int J Solids Struct 2013;50:1494–504.

[26] Drozdov AD, Christiansen JdeC, Stress–strain relations for hydrogels under multiaxial deformation. Int J Solids Struct 2013;50:3570–85.

[27] Bastide J, Candau S, Leibler L, Osmotic deswelling of gels by polymer solutions. Macromolecules 1981;14:719–26.

[28] Durning CJ, Morman Jr, KN, Nonlinear swelling of polymer gels. J Chem Phys 1993;98:4275–93.

[29] Okumura D, Kondo A, Ohno N, Using two scaling exponents to describe the mechanical properties of swollen elastomers. J Mech Phys Solids 2016;90:61–76.

[30] Gee G, The interaction between rubber and liquids. X. some new experimental tests of a statistical thermodynamic theory of rubber-liquid systems. Trans Faraday Soc 1946; 42:B033–B044.

[31] Okumura D, Mizutani M, Effects of two scaling exponents on swelling-induced softening of elastomers under equibiaxial and planar extensions. Key Eng Mater 2017;725:427–32.

[32] Bouklas N, Huang R, Swelling kinetics of polymer gels: comparison of linear and nonlinear theories. Soft Matter 2012;8:8194–203.